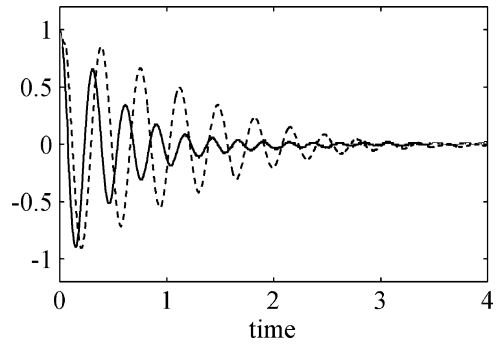

Fig. 22. Impulse responses (dashed line: type 2; solid line: type 3).

One is the use of a nonlinear elastic link. An example of such elasticity is one known for the TiNi shape memory alloy (SMA). When the strain is large, the maximum stress is limited. It is also known that elasticity and viscosity can be controlled by changing temperature of SMA. Adopting SMA as link material can be a promising approach to integrate a safety of the humanoid robot. The other is a joint design of active and passive compliance. By coupling these two compliances, we will obtain the appropriate compliance characteristic, which will be one of our future problems.

VIII. Conclusion

In this paper, we have proposed, designed and fabricated the new mechanism cybernetic shoulder for the humanoid robot shoulder.

1) The advantages of the cybernetic shoulder are compactness, large workspace, human-like motion, singularity free in the workspace and small backlash. And because of the closed kinematic chain, it is easy to introduce the mechanical compliance to the cybernetic shoulder.
2) We have discussed mathematics to solve the kinematics of the cybernetic shoulder.
3) We evaluate the human-like motion of the cybernetic shoulder by comparing with the human natural motion.
4) We can design the elasticity and the viscosity of the cybernetic shoulder by changing the material of link E which determines the kinematic constraints.
5) We have designed two types of new link E. One is $\phi 3$ mm carbon fiber link which has large compliance and small damping. The other is a $\phi 5$-mm carbon fiber link with a damper using Temper Foam.

References

[1] J. Yamaguchi and A. Takanishi, "Development of a biped walking robot having antagonistic driven joints using nonlinear spring mechanism," in *Proc. IEEE Int. Conf. Robotic Automation*, 1997, pp. 185–192.
[2] K. Hirai *et al.*, "The development of Honda humanoid robot," in *Proc. IEEE Int. Conf. Robotic Automation*, 1997, pp. 1321–1326.
[3] M. E. Rosheim, *Robot Evolution, The Development of Anthrobotics*. New York: Wiley , 1994.
[4] M. Inaba *et al.*, "A remort-brain full-body humanoid with multisensor imaging system of binocular viewer, ears, wrist force ant tactile sensor suit," in *Proc. Int. Conf. Robotic Automation*, 1997, pp. 2497–2502.
[5] A. E. Emgin and S. T. Tümer, "Three-dimensional kinematic modeling of the human shoulder complex—part I: physical model and determination of joint sinus cones," *ASME J. Biomech. Eng.*, vol. 111, pp. 107–121, 1989.
[6] I. A. Kapandji, *Physiologie Articulaire*, France: Maloine, 1980.
[7] J. Lenarčič and M. Stanišić, "A humanoid shoulder complex and the humanoid pointing kinematics," *IEEE Trans. Robot. Autom.*, vol. 19, no. 3, pp. 499–506, Jun. 2003.
[8] B. Hannaford, J. M. Winters, C. C. Chou, and P. H. Marbot, "The anthroform biorobotic arm: a system for the study of spinal circuits," *Ann. Biomed. Eng.*, vol. 23, pp. 399–408, 1995.
[9] W. Pollard, "Position controlling apparatus," U.S. Patent 2 286 571, Jun. 16, 1942.
[10] J. P. Trevelyan, "Skills for a shearing robot: dexterity and sensing," *Robot. Res.*, pp. 273–280, 1985.
[11] T. Yoshikawa and S. Kiriyama, "Four-joint redundant wrist mechanism and its control," *Trans. ASME J. Dyn. Syst. Meas. Control*, vol. 111, pp. 200–204, Jun. 1989.
[12] M. Rosheim, "In the footsteps of Leonardo," *IEEE Robot. Autom. Mag.*, vol. 4, no. 2, pp. 12–14, Jun. 1997.
[13] M. M. Stanišić and O. Duta, "Symmetrically acuated double pointing system: the basis of singularity-free robot wrists," *IEEE Trans. Robot. Autom.*, vol. 6, no. 5, pp. 562–569, Oct. 1990.
[14] S. J. Remis and M. M. Stanišić, "Design of a singularity-free articulated arm subassembly," *IEEE Trans. Robot. Autom.*, vol. 9, no. 6, pp. 816–824, Dec. 1993.
[15] M. M. Stanišić *et al.*, "A dexterous humanoid shoulder mechanism," *J. Robot. Syst.*, vol. 18, no. 12, pp. 737–745, 2001.
[16] R. Beyer, "Kinematische Getriebesynthese," in *Grundlagen einer quantitativen Getreibelehre ebener Getriebe, fr den Konstrukteur, die Vorlesung und das Selbststudium*. Berlin, Germany: Springer-Verlag, 1953.
[17] R. L. Willams, "Singularities of a manipulator with offset wrist," *ASME J. Mech. Des.*, vol. 121, no. 2, pp. 315–319, 1999.

Dimensional Design of Hexaslides for Optimal Workspace and Dexterity

A. B. Koteswara Rao, P. V. M. Rao, and S. K. Saha

***Abstract*—The paper presents the dimensional design of a class of parallel manipulators, namely, Hexaslides. The design of hexaslides is formulated as a multiobjective optimization problem considering workspace and dexterity as dual objectives. As the relative emphasis on workspace and dexterity varies depending on the application, a set of Pareto-optimal solutions is found. The present analysis is a useful tool for designers to select suitable hexaslide parameters for a given application, particularly, in machine tool applications.**

***Index Terms*—Dexterity, dimensional design, hexaslide, multi-objective optimization, workspace.**

I. Introduction

A general hexaslide manipulator consists of six distinct rails is shown in Fig. 1. The sliders move along the rail axes, whereas the legs of constant length are connected to the sliders through universal joints U_i for $i = 1$ to 6. The other end of each leg is connected to the tool or mobile platform through spherical joints indicated with B_i. Actuation of the sliders along their respective rail-axes drives the tool platform.

Manuscript received August 31, 2004. This paper was recommended for publication by Associate Editor J. Angeles and Editor I. Walker upon evaluation of the reviewers' comments.This work was supported by Gayatri Vidya Parishad College of Engineering, Visakhapatnam, and by the Indian Institute of Technology Delhi, India.

A. B. Koteswara Rao is with the Mechanical Engineering Department, Gayatri Vidya Parishad College of Engineering, Visakhapatnam 530 041, India (e-mail: abkr_iitd@yahoo.co.in).

P. V. M. Rao and S. K. Saha are with Mechanical Engineering Department, Indian Institute of Technology Delhi, Hauz Khas, New Delhi 110 016, India (e-mail: pvmrao@mech.iitd.ernet.in; saha@mech.iitd.ernet.in).

Digital Object Identifier 10.1109/TRO.2004.842353

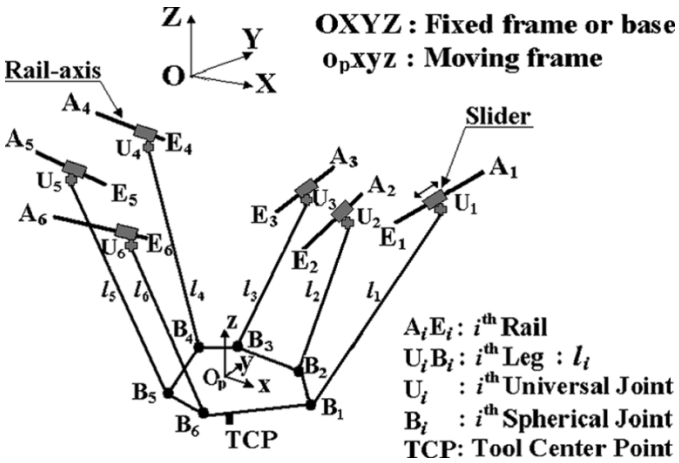

Fig. 1. General hexaslide machine tool.

As the main moving parts, namely, the legs, can be made light but stiff, the hexaslides find applications in machine tools, coordinate measuring machines, etc., where high accuracy and precision are required. Hexaglide [1] consisting of coplanar and parallel rails, HexaM [2] consisting of slanted rails, and Linapod [3] with the rails in vertical direction are three major machine tools based on hexaslides. These are all based on similar drive systems but with different rail arrangements.

In the design of hexaslide machine tools, the workspace and dexterity are considered two important performance indices. Workspace of a hexaslide is the space reachable by the tool while the dexterity is its ability to arbitrarily change its position and orientation, or apply forces and torques in arbitrary directions during machining. Complex workspace is one of the major drawbacks of the hexaslides. Moreover, the Jacobian matrix (J) that relates the actuated joint rates to the tool platform velocities is not constant and not isotropic; the performances vary considerably for different points in the workspace and for different directions at one given point. This is a serious drawback for the hexaslides to be used as machine tools [4], [5]. Hence, prior to the design of any hexaslide machine tool, it is necessary to identify suitable design parameters that offer the desired performance characteristics. In practice, relative emphasis on dexterity and workspace could vary depending on the application. Hexaslides that offer good workspace characteristics often perform poorly on dexterity front and vice versa. Hence, there is a need for addressing workspace and dexterity tradeoffs, in design of hexaslides, which has not been addressed so far. This has been attempted here by finding a set of nondominated hexaslides by multiobjective optimization [6], [7]. The workspace and dexterity related studies of hexaslides can be found from [8], [9], and others. However, there were no efforts made towards optimization and development of *Pareto-solutions*.

In this work, hexaslides having rails parallel by pairs and symmetrically arranged are considered for finding optimal workspace and dexterity. In the past [8], we made a comparison between the hexaslides with rails paired and unpaired. In both the cases, the rails are symmetrically arranged. It was observed that the hexaslides with rails parallel by pairs offer better workspace and dexterity. The same is evident from [10]. To describe general hexaslide geometry (Fig. 1) completely, 60 design variables are required. They are the three Cartesian coordinates of the start and end points of the rails (A_i and E_i) in the fixed frame O-XYZ, the center of spherical joints (B_i) in the moving frame $O_p - \mathrm{xyz}$, and the leg lengths l_i for $i = 1$ to 6. However, for a symmetric hexaslide with rails parallel by pairs, as shown in Fig. 2, only seven parameters are sufficient to describe it. These are R_b (radius of foot print circle on which the starting points of the rails lie), R_t (radius of tool platform), S (rail-length), L (leg length), G (gap between adjacent rails that are parallel), β (slant angle of rails with horizontal), and φ (separation angle between spherical joints on the tool platform).

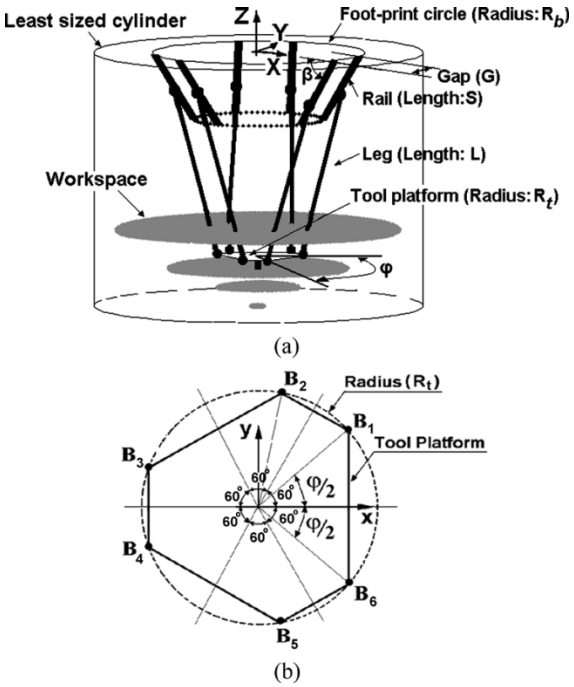

Fig. 2. Schematic diagram of a symmetric hexaslide with rails parallel by pairs. (a) Seven design parameters. (b) Spacing between spherical joints.

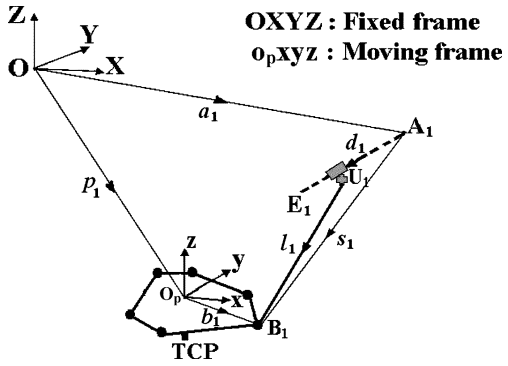

Fig. 3. Kinematic chain (for $i = 1$) of the hexaslide.

This paper is organized as follows. Section II presents the kinematic model of a general hexaslide, whereas some key performance measures are given in Section III. Section IV is presented with the optimization problem formulation with the results appearing in Section V. Finally, the conclusions are given in Section VI.

II. Kinematic Analysis

For the kinematic analysis, consider the loop $OA_1U_1B_1O_pO$ shown in Fig. 3, wherein O-XYZ is the fixed frame of reference attached to the base, $O_p - xyz$ is the moving frame attached to the tool platform, $\boldsymbol{p} \equiv \mathbf{OO_p} \equiv [p_x, p_y, p_z]^T$ is the position of center of the moving platform O_p in fixed frame, and R is the Rotation matrix representing the orientation of the moving frame $O_p - xyz$ with reference to O-XYZ. Now, for $i = 1$ to 6, l_i is the length of the ith leg, d_i is the distance of the ith slider from A_i, $S_i \equiv A_iE_i$ is the length of the ith rail, $\boldsymbol{u}_i$ is the unit vector along the ith rail, $\boldsymbol{a}_i \equiv \mathbf{OA}_i$, $\boldsymbol{d}_i \equiv \mathbf{A_iU_i}$, $\boldsymbol{l}_i \equiv \mathbf{U_iB_i} = l_i\boldsymbol{u}_i^l$, $\boldsymbol{s}_i \equiv \mathbf{A_iB_i}$, $\boldsymbol{b}_i \equiv \mathbf{O_pB_i}$ in moving frame. All the vectors except $\boldsymbol{b}_i$ are expressed in the fixed frame.

A. Position Analysis

From Fig. 3, $\boldsymbol{s}_i$, for $i = 1$ to 6, can be written as

$$\boldsymbol{s}_i = \boldsymbol{p} + R\,\boldsymbol{b}_i - \boldsymbol{a}_i, \quad \text{where } \boldsymbol{a}_i = \boldsymbol{d}_i + \boldsymbol{l}_i. \tag{1}$$

Since $\boldsymbol{d}_i = d_i \boldsymbol{u}_i$, (1) can be re-written as,

$$\boldsymbol{p} + R\,\boldsymbol{b}_i - \boldsymbol{a}_i - \boldsymbol{l}_i = d_i \boldsymbol{u}_i \tag{2}$$

or

$$(\boldsymbol{p} + R\,\boldsymbol{b}_i - \boldsymbol{a}_i - d_i\boldsymbol{u}_i)^T(\boldsymbol{p} + R\,\boldsymbol{b}_i - \boldsymbol{a}_i - d_i\boldsymbol{u}_i) = l_i^2. \tag{3}$$

The *inverse kinematic problem*, i.e., to find the position of actuators, d_i, for given $\boldsymbol{p}$ and R, can be solved using (3), i.e.,

$$\boldsymbol{d}_i = \left(\boldsymbol{s}_i^T\boldsymbol{u}_i\right) \pm \sqrt{(\boldsymbol{s}_i^T\boldsymbol{u}_i)^2 - (\boldsymbol{s}_i^T\boldsymbol{s}_i - l_i^2)}, \qquad \text{for } i = 1 \text{ to } 6. \tag{4}$$

Equation (4) offers two solutions, $d_i^{(1)}$ and $d_i^{(2)}$. The true solution can be identified based on the motion continuity, i.e., a given pose is achievable by the tool platform if the values of d_i satisfy the following constraint, alongwith the constraints imposed due to range of the motion allowed by the universal and spherical joints, namely

$$0 \le d_i \le S_i, \qquad \text{for } i = 1 \text{ to } 6. \tag{5}$$

B. Velocity Analysis

The time derivative of (2) yields

$$\dot{d}_i\boldsymbol{u}_i = \boldsymbol{v} + \boldsymbol{\omega} \times R\,\boldsymbol{b}_i - \boldsymbol{\omega}_i \times \boldsymbol{l}_i \tag{6}$$

where $\dot{d}_i$ is the linear speed of the i^{th} actuator, $\boldsymbol{v}$ and $\boldsymbol{\omega}$ are the three-dimensional (3-D) linear and angular velocities of the tool platform, and $\boldsymbol{\omega}_i$ is the angular velocity of the i^{th} leg. Taking the dot product of $\boldsymbol{l}_i$ on the both sides of (6), we get

$$\dot{d}_i\boldsymbol{u}_i^T\boldsymbol{l}_i = [\boldsymbol{v} + \boldsymbol{\omega} \times R\,\boldsymbol{b}_i]^T\boldsymbol{l}_i. \tag{7}$$

Equation (7) can be represented in the matrix form as

$$J_a\dot{\boldsymbol{d}} = J_t\boldsymbol{t}_p \tag{8}$$

where $\boldsymbol{t}_p \equiv [\boldsymbol{\omega}^T\ \boldsymbol{v}^T]^T$ is the six-dimensional (6-D) twist vector of the end effector, $\dot{d} \equiv [\dot{d}_1 \ldots \dot{d}_6]^T$, is the 6-D joint-rate vector, and the 6×6 matrices, J_a and J_t are given by

$$J_a \equiv \begin{bmatrix} \boldsymbol{l}_1^T\boldsymbol{u}_1 & & & 0 \\ & \cdot & & \\ & & \cdot & \\ & & & \cdot \\ 0 & & & \boldsymbol{l}_6^T\boldsymbol{u}_6 \end{bmatrix}$$

$$J_t \equiv \begin{bmatrix} (R\boldsymbol{b}_1 \times \boldsymbol{l}_1)^T & \boldsymbol{l}_1^T \\ \cdot & \cdot \\ \cdot & \cdot \\ \cdot & \cdot \\ (R\boldsymbol{b}_6 \times \boldsymbol{l}_6)^T & \boldsymbol{l}_6^T \end{bmatrix}. \tag{9}$$

Equation (8) may be re-written as

$$\dot{\boldsymbol{d}} = J\boldsymbol{t}_p \tag{10}$$

where the 6×6 Jacobian matrix, J, is expressed as

$$J \equiv J_a^{-1}J_t. \tag{11}$$

Note that J_a becomes singular when $\boldsymbol{l}_i^T\boldsymbol{u}_i = 0$, for any $i = 1$ to 6. This corresponds to *stationary singularity* [11]. In this type of singularity, the hexaslide loses one or more degree of freedom (DOF). When J_t becomes singular it refers to *uncertainty singularity* where the hexaslide gains one or more DOF.

III. Performance Measures

Among the measures of workspace the most commonly used one is the *constant-orientation workspace* [11], i.e., the 3-D Cartesian space reachable by the tool center point (TCP), while the orientation of the tool platform is constant. The determination of the exact workspace volume is indeed a difficult problem since the workspace boundary is defined by a set of highly nonlinear equations. In this paper, a simpler method, namely, the search method based on the inverse kinematics of Section II-A [12] is adopted. Search proceeds by defining a bounding box, say, 1.2 m$\times$1.2 m$\times$1.2 m, covering a maximum possible reachable space of a hexaslide, and then slicing the bounding box into a number of layers, e.g., 40, with each layer being discretized into points. For each of these points the distance, d_i in Fig. 3, is calculated and the constraints, (5), are checked. If the constraints are not violated, the point under computation is considered within the workspace, otherwise it is outside the workspace. The workspace volume is then computed as

$$\text{WSV} = \Sigma A_m \Delta z \tag{12}$$

where A_m is the reachable area in the $\boldsymbol{m}$th layer, and Δz is the layer interval. The non-dimensional indexes of workspace may be obtained by normalizing the workspace volume with either the cube of actuator stroke [13] or the hexaslide size [8]. In this paper, the *workspace volume index* (WVI), reported in [8], is used, which is obtained as

$$\text{WVI} = \left(\frac{\text{WSV}}{\text{Size of the Hexaslide}}\right) 100 \tag{13}$$

where the size of the hexaslide is the volume of the least sized cylinder enclosing the hexaslide and its workspace (Fig. 2).

Another index considered here is dexterity, which is defined as the condition number of the associated Jacobian matrix J, [14]. Geometrically, the Jacobian matrix, J, describes a hyperellipsoid having lengths defined by its singular values. The condition number represents the sphericity of the hyperellipsoid. The conditioning of J and the manipulability ellipsoid associated with J were used to optimize the workspace shape and performance uniformity of the Orthoglide [15]. An index that considers the dexterity of the manipulator over the entire workspace, namely, global dexterity index (GDI), [8], [16], and others, is given by

$$\text{GDI} = \frac{\int\limits_W \left\{\frac{1}{\kappa(J)}\right\} dW}{\int dW}. \tag{14}$$

In (14), dW is an infinitesimal small element representing one of the workspace points and $\kappa(J)$ is the condition number of the Jacobian matrix, J, at that point, which can be obtained using $\kappa(J) = \|J\|\|J^{-1}\|$, as reported in [16], in which $\|.\|$ refers to the Euclidean 2-norm. It may be noted that the evaluation of GDI requires inverse kinematics at each

point within the workspace, and consideration of constant-orientation to the tool platform, in the present work, yields unique value for $\kappa(J)$. Also, note that the ideal or least value of $\kappa(J)$ is unity referring to the isotropic condition. Hence, the more the GDI the more will be the uniformity in the kinematic performance characteristics.

It may be noted the first three columns of the Jacobian matrix, J of (11), have length units while the last three columns are dimensionless. This dimensional inhomogenity gives rise to inconsistencies while evaluating the GDI. Various approaches, to circumvent this problem, are reported in [14], [17], and others. In [9], [10], [14], and others, the first three columns of J are divided by the characteristic length (L_c) which leads to the definition of the normalized Jacobian matrix, J_n. Accordingly, the dexterity index GDI is modified as

$$\mathrm{GDI} = \frac{\int\limits_W \left\{\frac{1}{\kappa(J_n)}\right\} dW}{\int dW} \tag{15}$$

where $\kappa(J_n)$ is the condition number of the normalized Jacobian matrix at a point within the workspace that is computed as $\kappa(J_n) = \|J_n\|\|J_n^{-1}\|$. For the suitable choice of characteristic length, the GDI is evaluated using (15), taking $Lc = R_t$, R_b, L, and S. It has been observed that the GDI obtained with $L_c = R_t$ is maximum. So, R_t is chosen as the characteristic length.

IV. Optimization

The performance of a hexaslide depends highly on its architecture. It is always desirable to have both the workspace and dexterity values high. In the literature, very little work is traced in this direction. Majority of the researchers proposed optimum design procedures: 1) on dexterity, kinematic isotropy [18]; 2) on criterion with equal weightage to both the workspace and singularity [19] and 3) on a linear combination of dexterity measure and workspace index [13]. Mathematically, the optimization problem with multiple criteria or objectives may be stated [6] as

$$\begin{aligned} &\text{Maximize} \quad \mathbf{f} = [f_1(\mathbf{x}), f_2(\mathbf{x}), \ldots, f_m(\mathbf{x})] \\ &\text{subject to} \quad \mathbf{x} \in \boldsymbol{\Omega} \end{aligned} \tag{16}$$

where $\mathbf{x}$ is the vector of design variables, and $\boldsymbol{\Omega}$ is the feasible region or feasible set, and $f_i(\mathbf{x})$, for $i = 1$ to m, is the function of the ith objective. When there is a conflict between different criteria, it is important to have a global picture of the optimum solution(s), and the corresponding Pareto-set/front [6], [7]. A design variable vector $\mathbf{x}^* \in \boldsymbol{\Omega}$ is Pareto optimal for (16) if and only if there is no vector $\mathbf{x} \in \boldsymbol{\Omega}$ with the characteristics

$$f_i(\mathbf{x}) \geq f_i(\mathbf{x}^*) \quad \text{for all} \quad i, \qquad i = 1, 2, \ldots, m \tag{17a}$$

and

$$f_i(\mathbf{x}) > f_i(\mathbf{x}^*) \quad \text{for at least one} \quad i, \qquad i \in (1, m). \tag{17b}$$

The optimization problem is now formulated for the design of a hexaslide with the best possible WVI and GDI. The optimization problem for the design of hexaslides can be restated as

$$\begin{aligned} &\text{Maximize} \quad f(X) = g_1(\mathrm{WVI}) \\ &\text{subject to} \quad \bullet \text{ Design variable limits} \\ &\qquad\qquad \bullet \text{ Workspace constraints} \\ &\qquad\qquad \bullet \ \mathrm{GDI} \geq d_c \end{aligned} \tag{18}$$

TABLE I
Geometric Parameters of HexaM [21]

R_b (m)	S (m)	G (m)	β (deg.)	R_t (m)	φ (deg.)	L (m)
0.922	0.70	0.220	30.000	0.165	83.660	0.900

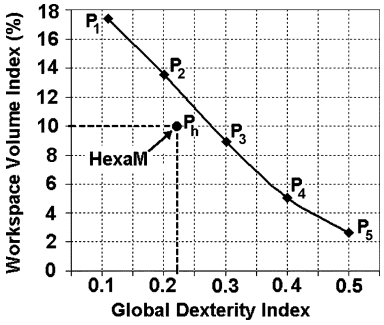

Fig. 4. Pareto-front of hexaslide machine tool for workspace and dexterity.

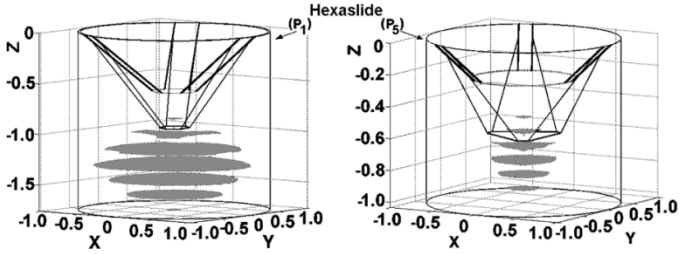

Fig. 5. Workspace relative to the size of hexaslide corresponding to P_1 and P_5.

and/or

$$\begin{aligned} &\text{Maximize} \quad f(X) = g_2(\mathrm{GDI}) \\ &\text{subject to} \quad \bullet \text{ Design variable limits} \\ &\qquad\qquad \bullet \text{ Workspace constraints} \\ &\qquad\qquad \bullet \ \mathbf{WVI} \geq w_c \end{aligned} \tag{19}$$

where g_1 and g_2 are the functions given by (13) and (15), respectively, whereas d_c and w_c are the lower limits on GDI and WVI, respectively. The Pareto-solutions are found, in the present work, from (18) and, or (19), using Sequential Quadratic Programming of MATLAB [20].

V. Results and Discussion

Evaluation of WVI and GDI, as described in the previous sections have been implemented in MATLAB. To validate the results of workspace and dexterity, an existing hexaslide machine tool, namely, the HexaM, is considered. The geometric parameters of HexaM [21], according to the notations shown in Fig. 2, are presented in Table I.

The results are obtained considering a suitable Cartesian bounding box of 1.2 m $\times$ 1.2 m $\times$ 1.2 m size and grid elements of 0.03 m $\times$ 0.03 m $\times$ 0.03 m size, from the MATLAB programs, as

$$\mathrm{WSV} = 0.327\ \mathrm{m}^3, \quad \mathrm{WVI} = 9.954\%, \quad \mathrm{GDI} = 0.222.$$

Note that the workspace volume computed here is same as that reported in [21]. The computation time for finding the WVI and GDI is 211 s on a 1.7 GHz, 256 MB RAM -P IV processor. To find a suitable grid size, during optimization, the WVI and GDI of the HexaM are found considering different grid sizes. Reduction in grid size increases the computation time drastically, with no significant changes in WVI and GDI.

TABLE II
PERFORMANCE INDICES FOR PARETO-SOLUTIONS OF HEXASLIDES AND CORRESPONDING PARAMETERS

Pareto points	GDI	WVI (%)	WSV (m^3)	R_b (m)	S (m)	G (m)	β (deg.)	R_t (m)	φ (deg.)	L (m)
P_1 (d_c = 0.1)	0.110	17.368	0.966	1.000	0.991	0.264	36.568	0.163	76.063	1.179
P_2 (d_c = 0.2)	0.201	13.521	0.640	1.000	0.863	0.259	32.827	0.230	92.950	1.053
P_3 (d_c = 0.3)	0.302	8.944	0.370	1.000	0.766	0.248	31.813	0.280	100.522	0.942
P_4 (d_c = 0.4)	0.400	5.007	0.183	1.000	0.627	0.234	30.238	0.349	103.706	0.898
P_5 (d_c = 0.5)	0.500	2.649	0.086	1.000	0.525	0.144	28.378	0.413	107.159	0.878

d_c: Limit or constraint imposed over the Global Dexterity Index during the optimization for Workspace Volume Index

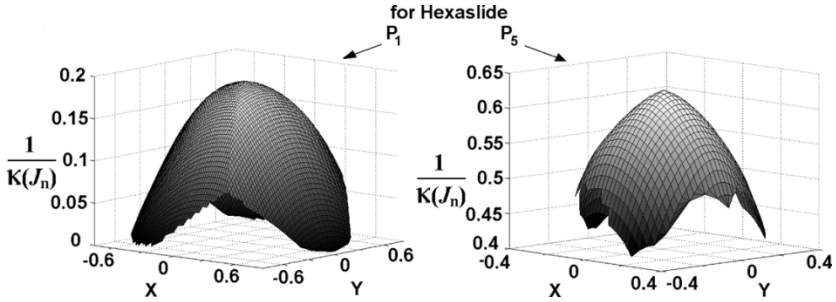

Fig. 6. Variation of reciprocal of Jacobian condition number within the central horizontal plane of the workspace of typical hexaslides.

For the estimation of WVI and GDI during the optimization, a grid of 0.04 m $\times$ 0.04 m $\times$ 0.03 m is used as this offers error in the evaluation of both WVI and GDI is less than 0.1%. Details are not reported due to the space limitation. Now obtaining typical nondominated hexaslides, of HexaM type, is presented. For the multiobjective optimization, the sequential quadratic programming (SQP) method is adopted wherein the QP subproblem is solved at each iteration. A critical issue to obtain an optimum design solution is the choice of a proper initial guess. The optimality of the obtained solutions was confirmed by implementing the optimization algorithms a number of times from different initial solutions.

Considering the constraint over the GDI, i.e., $d_c = 0.1$ in (18), hexaslides offering maximum WVI is found. The point, P_1, in Fig. 4, in the Pareto-front corresponds to the values in first row of Table II. As the relative emphasis on workspace and dexterity vary depending on an application, the optimization experiments are continued to find some other Pareto-points by imposing constraints on the GDI values. The corresponding points are P_2, P_3, P_4, and P_5 of Fig. 4, where $d_c = 0.2, 0.3$, 0.4, and 0.5, respectively. Optimization results are presented in Table II. It may be noted that all the length parameters of hexaslides reported in Table II are normalized by taking $R_b = 1.0$ m. In Fig. 4, $P_{\rm h}$ represents the WVI and GDI of the HexaM. Note here that when the priority on workspace is high the hexaslide corresponding to the Pareto-point P_1 is suitable as it offers highest WVI, namely, $\mathrm{WVI} = 17.37\%$, while GDI is lowest, i.e., $\mathrm{GDI} = 0.11$. On the other hand, when the highest dexterity is preferred, the hexaslide corresponding to the Pareto-point P_5 should be chosen as it offers highest GDI $(= 0.5)$ and lowest WVI $(= 2.65\%)$. Thus, a gain of 14.72% in WVI is expected with a reduction in the GDI value by 0.39, and vice versa. Though the hexaslides corresponding to the Pareto-points P_3, P_4, and P_5 offer less WVI when compared to the HexaM, these are superior in terms of the dexterity. On the contrary, the hexaslides corresponding to the Pareto-points P_1 and P_2 offer less dexterity when compared to the HexaM but are superior with respect to the WVI. The workspaces offered by two hexaslides that correspond to the Pareto-points, P_1 and P_5, are shown in Fig. 5. The lower and higher dexterity for P_1 and P_5, respectively, are quite obvious from Fig. 6, where variations of the reciprocal of the condition number of Jacobian matrix, i.e., $[1/\kappa(J_{[}n)]$, are shown within the central horizontal section of the workspaces.

As the dexterity requirements are high in case of a class of Machine Tools such as Tool and Cutter Grinder due to the complex kinematic motions, the hexaslide corresponding to Pareto-point P_5 should be considered. On the contrary, the workspace is primary interest in 3 axis Milling and, hence, the hexaslide corresponding to Pareto-point P_1 is suitable. Other observations are: 1) smaller gap between the rails offer better dexterity but adversely affects the workspace; 2) longer rails and legs offer larger workspace with less dexterity and 3) larger tool platforms offer high dexterity and less workspace.

VI. CONCLUSION

Kinematic modeling and analyses, and the dimensional design of hexaslides are presented. The key contributions are as follows.

- Multi-objective optimization of hexaslides was carried out with dexterity and workspace as dual objectives.
- All the seven design variables that are necessary for the complete description of the symmetric hexaslides with rails parallel by pairs were considered;
- As the relative emphasis on workspace and dexterity vary for different class of Machine Tools, a set of nondominated hexaslides, are obtained.
- The nearness to HexaM in the centre of Pareto-front confirms its equal emphasis on workspace and dexterity.

The methodology proposed, and the results reported in this work are useful for the selection of a suitable hexaslide. Further research on the optimum design of hexaslides including the stiffness and the orientation workspace is underway and will be the subject of future correspondences.

REFERENCES

[1] M. Honegger, A. Codourey, and E. Burdet, "Adaptive control of the hexaglide, a 6 DOF parallel manipulator," in *Proc. IEEE Int. Conf. on Robotics and Automation*, Albuquerque, 1997, pp. 543–548.

[2] M. Suzuki, K. Watanabe, T. Shibukawa, T. Tooyama, and K. Hattori, "Development of milling machine with parallel mechanism," *Toyota Tech. Rev.*, vol. 47, no. 1, pp. 125–130, 1997.
[3] G. Pritschow and K. H. Wurst, "Systematic design of hexapods and parallel link systems," *Ann. CIRP*, vol. 46, no. 1, pp. 291–295, 1997.
[4] P. Wenger, C. Gosselin, and B. Maille, "A comparative study of serial and parallel mechanism topologies for machine tools," in *Proc. PKM'99*, Milan, Italy, 1999, pp. 23–32.
[5] T. Treib and O. Zirn, "Similarity laws of serial and parallel manipulators for machine tools," in *Proc. 4th Int. Conf. Motion and Vibration Control—MOVIC'98*, Zurich, Switzerland, Aug. 25–28.
[6] D. B. Ashok and R. C. Tirupathi, *Optimization Concepts and Applications in Engineering*. New Delhi, India: Pearson, 2002.
[7] O. Andrezj, *Multicriterion Optimization in Engineering*. Chichester, U.K.: Ellis Horwood, 1984.
[8] A. B. Koteswara Rao, P. V. M. Rao, and S. K. Saha, "Workspace and dexterity analyses of hexaslide machine tools," in *Proc. IEEE Int. Conf. on Robotics and Automation*, Taipei, Taiwan, R.O.C., 2003, pp. 4104–4109.
[9] F. Xi, "A comparison study on hexapods with fixed-length legs," *Int. J. Machine Tools Manufact.*, vol. 41, pp. 1735–1748, 2001.
[10] J. Ryu and J. Cha, "Volumetric error analysis and architecture optimization for accuracy of hexaslide type parallel manipulators," in *Mech. Mach. Theory*, 2003, vol. 38, pp. 227–240.
[11] J. P. Merlet, *Parallel Robots*. Dordrecht, The Netherlands: Kluwer, 2000.
[12] O. Masory and J. Wang, "Workspace evaluation of Stewart platforms," *Adv. Robot.*, vol. 9, no. 4, pp. 443–461, 1995.
[13] R. S. Stoughton and T. Arai, "A modified Stewart platform manipulator with improved dexterity," *IEEE Trans. Robot. Autom.*, vol. 9, no. 2, pp. 166–173, Apr. 1993.
[14] C. Gosselin, "Dexterity indexes for planar and spatial robotic manipulators," in *Proc. IEEE Int. Conf. Robotics and Automation*, 1990, pp. 650–655.
[15] P. Wenger and D. Chablat, "Design of a three axis isotropic parallel manipulator for machining applications: The Orthoglide," in *Proc. Workshop on Fundamental Issues and Future Research Directions for Parallel Mechanisms and Manipulators*, Québec City, QC, Canada, 2002, pp. 16–24.
[16] C. Gosselin and J. Angeles, "A global performance index for the kinematic optimization of robotic manipulators," *ASME Int. J. Mech. Des.*, vol. 113, no. 3, pp. 220–226, 1991.
[17] J. Angeles, F. Ranjbaran, and R. V. Patel, "On the design of the kinematic structure of 7 axis redundant manipulators for maximum conditioning," in *Proc. IEEE Int. Conf. on Robotics and Automation*, 1992, pp. 494–499.
[18] K. E. Zanganeh and J. Angeles, "Kinematic isotropy and the optimum design of parallel manipulators," *Int. J. Robot. Res.*, vol. 16, no. 2, pp. 185–197, 1997.
[19] E. Ottaviano and M. Ceccarelli, "Optimum design of parallel manipulators for workspace and singularity performances," in *Proc. Workshop Fundamental Issues and Future Research Directions for Parallel Mechanisms and Manipulators*, Québec City, QC, Canada, 2002, pp. 98–105.
[20] The Math Works, Optimization Toolbox for Use With Matlab, 2000.
[21] I. A. Bonev and J. Ryu, "Workspace analysis of 6-PRRS parallel manipulators based on the vertex space concept," in *Proc. ASME Design Engg. Tech. Conf.*, 1999, DETC 99/DAC-8647.

Conceptual Design and Dimensional Synthesis for a 3-DOF Module of the TriVariant—A Novel 5-DOF Reconfigurable Hybrid Robot

T. Huang, M. Li, X. M. Zhao, J. P. Mei, D. G. Chetwynd, and S. J. Hu

***Abstract*—This paper deals with the conceptual design and dimensional synthesis of a 3-DOF parallel mechanism module which forms the main body of a newly invented 5-DOF reconfigurable hybrid robot named "TriVariant." The TriVariant is a modified version of the Tricept robot, achieved by integrating one of the three active limbs into the passive limb. The idea leading to the innovation of the module is systematically addressed. Its kinematic performance is optimized by minimizing a global and comprehensive conditioning index subject to a set of appropriate mechanical constraints. It is concluded that the proposed hybrid system is more cost-effective and has a competitive kinematic performance in comparison with the well-known Tricept robot.**

***Index Terms*—Conceptual design, dimensional synthesis, parallel kinematic machines (PKMs), reconfigurable manufacturing.**

I. Introduction

Parallel kinematic machines (PKMs) have drawn continuous interest in both industry and academia in the machine tool/robot sectors since the 1990s because of their potentially desirable fast dynamic performance, rigidity, and acceptable accuracy. It was clearly indicated that one of the future trends toward the PKM development is to make full use of its reconfigurability and multiple functionality [1]. Indeed, characterized by the multiple closed-loop kinematic chains with identical components, the PKM concept would most likely lead to the standardization of drive units, joints, and interfaces within a machine and thereby enable the generation of a special class of reconfigurable machine tools/robots [2]–[5].

Although numerous PKMs with different architectures have been developed previously [6] (the well-known Hexapods, Hexaglide, and Delta, for example), few of them really possess true reconfigurability because of the limited modularization at the component level. Here, "reconfigurability" means the capability to form a multi-axis, multifunctional, and plug-and-play module that can then be used to configure different machines. In this sense, the Tricept robot [see Fig. 1(a)] with parallel-serial architecture stands out [7], with its high dynamics, rigidity, and large workspace/footprint ratio. Today, various versions of the Tricept have been successfully used as machine tools and/or robots

Manuscript received June 16, 2004; revised October 11, 2004. This paper was recommended for publication by Associate Editor Z. X. Li and Editor F. Park upon evaluation of the reviewers' comments. This work was supported in part by the National Science Foundation of China under Grant 50328506 and Grant 50375106, the Royal Society U.K.–China Exchange under Grant Q820, the Ministry of Education of China under Grant 20020056027, and Tianjin Science and Technology Commission.

T. Huang is with the School of Mechanical Engineering, Tianjin University, Tianjin 300072, China, and also with the University of Warwick, Coventry CV4 7AL, U.K. (e-mail: htiantju@public.tpt.tj.cn).

M. Li, X. M. Zhao, and J. P. Mei are with the School of Mechanical Engineering, Tianjin University, Tianjin 300072, China (e-mail: limengli@public.tpt.tj.cn; zxm@tju.edu.cn; mjp@tju.edu.cn).

D. G. Chetwynd is with the School of Engineering, the University of Warwick, Coventry CV4 7AL, U.K. (e-mail: D.G.Chetwynd@warwick.ac.uk).

S. J. Hu is with the Department of Mechanical Engineering, University of Michigan, Ann Arbor, MI 48190 USA (e-mail: jackhu@umich.edu).

Digital Object Identifier 10.1109/TRO.2004.840908